J. Fluid Mech. (2008), *vol.* 606, *pp.* 133–151.
doi:10.1017/S0022112008001638 Printed in the United Kingdom

An experimental study of kicked thermal turbulence

XIAO-LI JIN AND KE-QING XIA

Department of Physics, The Chinese University of Hong Kong, Shatin, Hong Kong, China

(Received 14 August 2007 and in revised form 19 March 2008)

We present an experimental study of turbulent Rayleigh–Bénard convection (RBC) in which the input energy that drives the turbulent flow is in the form of periodical pulses. A surprising finding of the study is that in this 'kicked' thermal turbulence the heat transfer efficiency is enhanced compared to both constant and sinusoidally modulated energy inputs. For the apparatus used in the present study, an enhancement of 7% of the dimensionless Nusselt number Nu has been achieved. The enhancement is found to depend on two factors. One is the synchronization of the kicking period of energy input with the intrinsic time scale of the turbulent flow. When the repetition period of the input energy pulse equals half of the large-scale flow turnover time, a resonance or optimization of the enhancement is achieved. The other factor is the pulse shape (the inverse square of the energy input duty cycle). We find that a spiky pulse is more efficient for heat transfer than a flatter one of the same energy. It is found that in this kicked thermal turbulence there exist appropriate ranges of the kicking strength A and the kicking frequency f in which the Rayleigh number Ra grows to a saturation level and that the saturated Ra fluctuates between a lower saturation level Ra_l^{sat} and an upper saturation level Ra_u^{sat}. For large enough saturated Ra, power-law dependences on f and A are found: $Ra_l^{sat} \propto (Af)^{0.80\pm0.02}$ and $Ra_u^{sat} \propto f^{0.70\pm0.01}A^{0.84\pm0.02}$. The scaling law for Ra_l^{sat} is found to agree quantitatively with the prediction of a mean-field theory of kicked turbulence (Lohse, *Phys. Rev.* E vol. 62, 2000, p. 4946) when the latter is appropriately extended to the case of kicked thermal turbulence. It is further found that a large-scale circulatory flow (LSC) still exists in the kicked RBC, and that its Reynolds number has the same scaling with Ra as in the steadily driven case, i.e. $Re_f \propto Ra^{0.46\pm0.01}$. The present study provides an example of achieving enhanced heat transfer in a convective system by first triggering the emission of clustered thermal plumes via an active control and then synchronizing the transport of the plume clusters with an internal time scale.

1. Introduction

Turbulent flows driven by time-dependent forcing abound in nature and in industrial applications. One can readily think of many examples such as the Earth's atmosphere driven by periodical heating from the sun's radiation, the tidal ocean current induced by periodical gravitational attractions of the moon and the sun, the blood flow in veins driven by the beat of the heart, and the flow in the intake of combustion engines driven by the piston. However, despite its ubiquity, periodically driven flows have attracted relatively little attention.

In recent years, a series of works has focused on the effect of the external time-dependent forcing on the global properties of the turbulent system. Two specific types

of time-dependent forcing have been theoretically studied. One uses periodical pulses as energy inputs to drive turbulent flow. Lohse (2000) studied this periodically 'kicked' turbulence in shear flows using a mean-field theory. The effect of kicked forcing on the time evolution of the Reynolds number was analysed. He showed that the Reynolds number will first grow and then reach a saturation level determined by the kicking strength and kicking frequency. Some of these theoretical results were numerically verified later using a Gledzer–Ohkitani–Yamada (GOY) shell model (Hooghoudt, Lohse & Toschi 2001). However, to our knowledge, no experimental investigation has been conducted using periodically kicked forcing in any type of flow.

The other forcing type is the sinusoidal modulation of the energy input rate on the outer length scale of the turbulent system. Heydt, Grossmann & Lohse (2003*a*) studied the response of a turbulent system to a weak modulation of the energy input rate using a mean-field theory. They predicted that the response is dependent on the relationship between the modulation frequency and the energy cascade frequency scale. For low driving frequencies the system follows the modulation with almost constant amplitude while for higher frequencies the response amplitude decreases inversely with the modulation frequency. Subsequent numerical simulation using a GOY shell model and a reduced wave vector set approximation (REWA) (Heydt, Grossmann & Lohse 2003*b*), and direct numerical simulation (DNS) (Kuczaj, Geurts & Lohse 2006) reported similar results. The theoretical results of Heydt *et al.* (2003*a*) have been verified by Cadot, Titon & Bonn (2003) in an experiment conducted in a closed geometry between two counter-rotating disks.

In this paper, we present an experimental study of periodically kicked turbulence in a Rayleigh–Bénard convection cell. To the best of our knowledge, this is the first attempt to study the effect of this specific type of forcing in a precisely controlled experimental system. The steadily driven Rayleigh–Bénard convection (RBC) has been studied extensively in the past two decades. The state of fluid motion in the system is characterized by three control parameters, namely the Rayleigh number $Ra(=\alpha g\Delta H^3/\nu\kappa)$, the Prandtl number $Pr(=\nu/\kappa)$, and the aspect ratio $\Gamma(=D/H)$, where Δ is the applied temperature difference across a fluid layer of height H and lateral dimension D, g is the gravitational acceleration, and α, ν, and κ are, respectively, the volume expansion coefficient, kinematic viscosity, and thermal diffusivity of the convecting fluid. Two important response parameters can also be defined: the Nusselt number $Nu(=J/(\chi\Delta/H))$, which is the ratio of the effective thermal conductivity of the convecting fluid to the conductivity of the quiescent fluid; and the Reynolds number $Re(=UH/\nu)$. Here χ is the thermal conductivity of the fluid, J is the heat flux across the fluid layer, and U is a typical velocity scale of the convective flow.

The remainder of this paper is organized as follows. The experimental setup will be described in § 2. The experimental results of the Rayleigh number response, local temperature fluctuations, the large-scale circulation, and Nusselt number enhancement will be presented and discussed in §§ 3.1–3.4, respectivley. In § 3.5, we present a version of Lohse's mean-field theory modified for the case of kicked thermal turbulence and compare its results with our experimental findings.

2. Experiment

The experiment was conducted in two upright cylindrical cells filled with water ($Pr \simeq 4.3$). The two convection cells have the same inner diameter of $D = 19.4$ cm and different heights H of 19.4 cm and 39.2 cm. The corresponding aspect ratios of the

two cells are therefore $\Gamma = 1$ and $\Gamma = 0.5$, respectively. Details about the apparatus have been described elsewhere (Shang & Xia 2001) and here we mention only some of its essential features. The upper and lower plates are made of copper and the sidewall is a transparent Plexiglas tube. In the experiment, a program-controlled power supply is used to heat the lower plate, so that a pulsed heating can be imposed on the system. The upper plate is cooled by a refrigerated recirculator at a constant temperature. During the experiment the entire convection cell was wrapped by several layers of thermal insulating material and placed in a thermostat box with a temperature set at the mean temperature (40°C) of the convecting fluid. The thermostat box has a temperature stability of 0.05°C.

Five thermistors with 2.4 mm diameter, 1 s time constant, and 0.005°C accuracy are embedded in the upper and lower plates to probe the local temperature in the plate. Three are placed in the lower plate along a diameter, one being at plate centre and the other two at mid-radius from the plate centre, and all are 0.5 mm from the fluid-contact surface. The other two thermistors are placed in the upper plate, opposite to each other, at mid-radius from the plate centre and are 1.5 mm from the fluid-contact surface. The typical sampling rate for the plate temperature measurement is between 0.5 and 1 Hz. In addition, two smaller thermistors with 0.2 mm diameter, 15 ms response time, and 20 mK/Ω temperature sensitivity are placed inside the cell to probe local temperatures in the convecting fluid, one at the cell centre and the other near the sidewall at mid-height. The sampling rate for measurements in the fluid varies from 8 to 64 Hz, depending on the value of Ra. During the experiment the cell was tilted by a small angle so that the large-scale circulatory flow was locked in the vertical plane that contains the sidewall thermistor.

At time $t = 0$, the pulsed heating power is imposed on the lower plate. The local temperature time series are measured, from which Rayleigh number and Nusselt number are obtained. Different values of Ra and Nu had been achieved by varying three pulse parameters: the pulse width Δt_{kick}, the separation time Δt between adjacent pulses, and the pulse height P. Although the experiments were conducted by varying the above pulse parameters, most of the results shown below are presented in terms of an alternative set of three parameters (Lohse 2000): the kicking frequency $f = 1/\Delta t$, kicking strength $A = P\Delta t_{kick}$ (which is just the energy of the pulse), and the pulse repetition period $T_{kick} = \Delta t + \Delta t_{kick}$. For each set of pulse parameters, a corresponding constant heating experiment with the same average heating power $P_c = P\Delta t_{kick}/(\Delta t_{kick} + \Delta t)$ is also performed for comparison.

3. Results and discussion

3.1. *Rayleigh number response*

Figure 1(*a*) shows the time series of Ra measured in the $\Gamma = 1$ cell for a fixed kicking strength $A = 347.66$ J and various kicking frequencies f, from bottom to top, 5×10^{-4} Hz, 3.36×10^{-3} Hz, 1.13×10^{-2} Hz, 3.33×10^{-2} Hz, 1.25×10^{-1} Hz, and 3.33×10^{-1} Hz. For clarity, a segment of saturated $Ra(t)$ measured with $f = 0.033$ Hz is shown in figure 1(*b*). Here $Ra(t)$ is obtained based on the instantaneous temperature difference $\Delta T(t) = T_b(t) - T_t(t)$ between the plates, where the bottom plate temperature $T_b(t)$ is the arithmetic mean of the readings from the three thermistors imbedded in the bottom plate and $T_t(t)$ is that based on the readings from the two thermistors imbedded in the top plate. The figure clearly shows that during each pulsed heating cycle there is a kick and a subsequent decay in Rayleigh number. Overall, there is growth up to some saturation level Ra^{sat} when the kicking frequency f is larger than

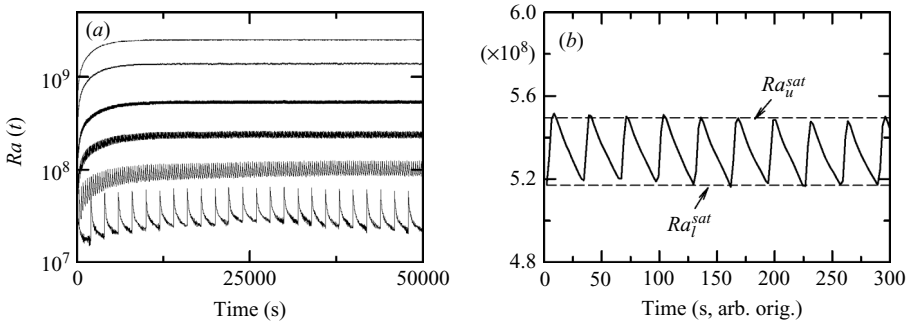

FIGURE 1. (*a*) Time evolution of Ra measured in the $\Gamma = 1$ cell for a fixed kicking strength $A = 347.66$ J, and various kicking frequencies, from bottom to top, $f = 5\times10^{-4}$ Hz, 3.36×10^{-3} Hz, 1.13×10^{-2} Hz, 3.33×10^{-2} Hz, 1.25×10^{-1} Hz, and 3.33×10^{-1} Hz. (*b*) A segment of saturated $Ra(t)$ measured with $A = 347.66$ J and $f = 0.033$ Hz (the fourth curve from the bottom shown in (*a*)). The dashed lines denote the lower saturation level Ra_l^{sat} and the upper saturation level Ra_u^{sat}.

3.36×10^{-3} Hz in our system. The saturated $Ra(t)$ is seen to fluctuate between a lower saturation level Ra_l^{sat} and an upper saturation level Ra_u^{sat}, which are obtained respectively by averaging the individual peaks and valleys of the saturated $Ra(t)$. It is also seen that, as f increases, the saturation level increases but the difference between the lower and upper saturation levels decreases. For low kicking frequency there is almost no overall growth to the saturation level, as the excitation caused by the kick always returns to the initial level after decay. In his mean-field theory of kicked turbulence for shear flows, Lohse (2000) has predicted that, for appropriate values of A and f, the Reynolds number Re will grow up to some saturation level and then fluctuate between a lower saturation level Re_l^{sat} and an upper saturation level Re_u^{sat} when the energy input during Δt_{kick} balances energy loss during Δt. As we will show in § 3.3, a power-law relationship between Ra and Re still holds in kicked thermal turbulence, which means Ra and Re should exhibit similar qualitative behaviour. Thus the above measured properties of the Rayleigh number verify the first prediction of the Lohse theory.

In figure 2 we examine the dependence of the saturated Ra on the kicking frequency f and kicking strength A. The upper panels show data measured in the $\Gamma = 1$ cell and the lower panels are those in the $\Gamma = 0.5$ cell. Figure 2(*a*) shows in log-log scale Ra_l^{sat} and Ra_u^{sat} as functions of f for two different kicking strengths $A = 347.66$ J and 1008 J. It is clear that there exists power-law dependence for f above certain value. The figure also shows that as f decreases the difference between Ra_l^{sat} and Ra_u^{sat} increases. Also, when f becomes smaller than $\sim10^{-3}$, the power-law behaviour breaks down. The non-power-law regime corresponds to those values of Ra that cannot achieve a saturation state as shown in figure 1(*a*). Figure 2(*b*) shows the log-log plot of Ra_l^{sat} and Ra_u^{sat} as functions of A for two different kicking frequencies $f = 0.033$ Hz and 0.0034 Hz. The figure also shows that a power-law behaviour emerges when f and/or A are larger than some value. If we examine the corresponding Ra^{sat} in both figures 2(*a*) and 2(*b*), it is seen that the values of A and f that produce power-law behaviour also give rise to $Ra^{sat} \gtrsim 10^8$. Therefore, the kicked convective flow may be regarded as in the turbulent regime when Ra^{sat} is above this value. The dashed lines show power-law fits to those data points with Ra^{sat} above $\sim10^8$.

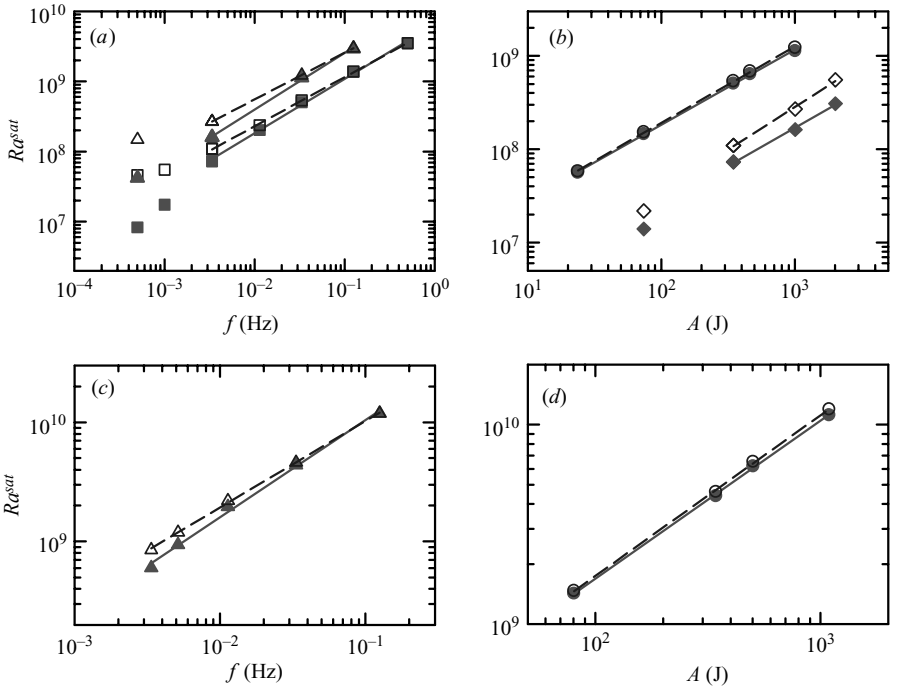

FIGURE 2. Log-log plots of the lower saturation level Ra_l^{sat} (solid symbols) and the upper saturation levels Ra_u^{sat} (open symbols) versus the kicking frequency f (a, c) and the kicking strength A (b, d), respectively. Data measured for (a) two values of $A = 347.66$ J (triangles) and 1008 J (squares); (b) two values of $f = 0.033$ Hz (circles) and 0.0034 Hz (diamonds); (c) a fixed $A = 347.66$ J (triangles); (d) a fixed $f = 0.033$ Hz (circles). The upper panels (a, b) are data measured in the $\Gamma = 1$ cell and lower panels (c, d) those from the $\Gamma = 0.5$ cell. Lines are power-law fits.

	$\Gamma = 1$		$\Gamma = 0.5$	
	Ra_l^{sat}	Ra_u^{sat}	Ra_l^{sat}	Ra_u^{sat}
$A = 347.7$ J	$f^{0.78\pm0.02}$	$f^{0.70\pm0.01}$	$f^{0.82\pm0.03}$	$f^{0.73\pm0.01}$
$A = 1008$ J	$f^{0.81\pm0.04}$	$f^{0.67\pm0.01}$	—	—
$f = 0.033$ Hz	$A^{0.81\pm0.01}$	$A^{0.82\pm0.01}$	$A^{0.79\pm0.01}$	$A^{0.80\pm0.01}$
$f = 0.0034$ Hz	$A^{0.81\pm0.05}$	$A^{0.91\pm0.05}$	—	—

TABLE 1. The best power-law fits to data points in figure 2.

Figures 2(c) and 2(d) show, respectively, *Ra vs f* and *Ra vs A* relationships measured in the $\Gamma = 0.5$ cell, for which only one set of scans for each parameter was made. For this cell, the lowest Ra^{sat} is around 10^9, so all data points appear to fall within the scaling regime. The data otherwise show similar properties as those measured in the $\Gamma = 1$ cell. In table 1 we list the best power-law fits to the data points.

Summarizing results for both $\Gamma = 1$ and $\Gamma = 0.5$ cells, we conclude that there is a power-law dependence of Ra_l^{sat} and Ra_u^{sat} on kicking frequency f and kicking strength A for large enough saturated Ra ($\gtrsim 10^8$). Because of the relatively narrow scaling range, there are some variations in the scaling exponents. By averaging the exponents of Ra_l^{sat} (Ra_u^{sat}) with f for different values of A and Γ, and the exponents of Ra_l^{sat} (Ra_u^{sat}) with A for different value of f and Γ, respectively, we have the following results:

$$Ra_l^{sat} \propto (fA)^{0.80\pm0.02}, \tag{3.1}$$

$$Ra_u^{sat} \propto f^{0.70\pm0.01} A^{0.84\pm0.02}. \tag{3.2}$$

For the lower saturation level Ra_l^{sat}, the power-law dependence on f and A give the same exponent. Thus Ra_l^{sat} scales as the product of Af. For the upper saturation level Ra_u^{sat}, the power-law dependence on f and A give different exponents. However, the two exponents are close to each other. Therefore, the above result also verifies another prediction of Lohse's mean-field theory that the saturated Ra in the turbulent regime scales as the product of Af. However, as the theory was developed for plane shear flows the predicted scaling exponents are different from the present case. In § 3.5 we will present a modified version of Lohse's mean-field theory for the case of kicked thermal turbulence and make a more quantitative comparison.

3.2. *Local temperature fluctuations*

To quantify the temperature fluctuations in kicked thermal turbulence, standard deviations of temperature signals are measured. Data for corresponding constant-heating cases are also taken for comparison. We use σ_b, σ_t, σ_c and σ_s to represent the standard deviations of temperature fluctuations in the bottom plate, the top plate, the cell centre and the sidewall, respectively. Superscripts $^{(k)}$ and $^{(c)}$ denote kicked and constant-heating cases respectively. Figures 3(*a*), 3(*b*), 3(*c*), and 3(*d*) respectively show σ_b, σ_t, σ_c, and σ_s as functions of Ra. The results measured in the kicked and constant-heating cases are plotted in the same figure for comparison.

For constant heating, the dependence of σ on Ra at different positions can be fitted by power laws: $\sigma_b^{(c)} \sim Ra^{0.84\pm0.01}$, $\sigma_t^{(c)} \sim Ra^{0.91\pm0.01}$, $\sigma_c^{(c)} \sim Ra^{0.87\pm0.01}$, $\sigma_s^{(c)} \sim Ra^{0.73\pm0.01}$. These results are similar to those recently reported by Sun & Xia (2007). The fact that local temperature fluctuations measured inside the conducting plates have similar power-law exponents to those measured in the cell interior suggests that they are dominated by signatures of stochastic turbulent fluctuations in the convective flow. It is also known that signals related to thermal plumes constitute an important part of these fluctuations (Sun & Xia 2007). Figure 3 also shows that for a given Ra the magnitudes of temperature fluctuations measured inside the plates and at cell centre are of the same order while that measured near the sidewall is about one order larger. This is consistent with the fact that thermal plumes are predominantly transported in the sidewall region (Shang *et al.* 2003; Xi, Lam & Xia 2004).

For the pulsed heating case, the $\sigma_b^{(k)}$ *vs* Ra relationship has a transition at $Ra \sim 2 \times 10^9$ (figure 3*a*). When Ra is below this transition point, $\sigma_b^{(k)}$ may be regarded as constant within experimental uncertainties and there is a large difference between $\sigma_b^{(k)}$ and $\sigma_b^{(c)}$. When Ra is above the transition point, $\sigma_b^{(k)}$ increases as Ra increases and it begins to overlap with $\sigma_b^{(c)}$. For $\sigma_t^{(k)}$ (figure 3*b*) and $\sigma_c^{(k)}$ (figure 3*c*), similar properties can be found. However, the value of the transition Ra ($\sim 2 \times 10^8$) is much lower than that for $\sigma_b^{(k)}$. For temperature fluctuations near the sidewall (figure 3*d*), $\sigma_s^{(k)}$ and $\sigma_s^{(c)}$ almost coincide with each other. Only small differences exist at low Ra.

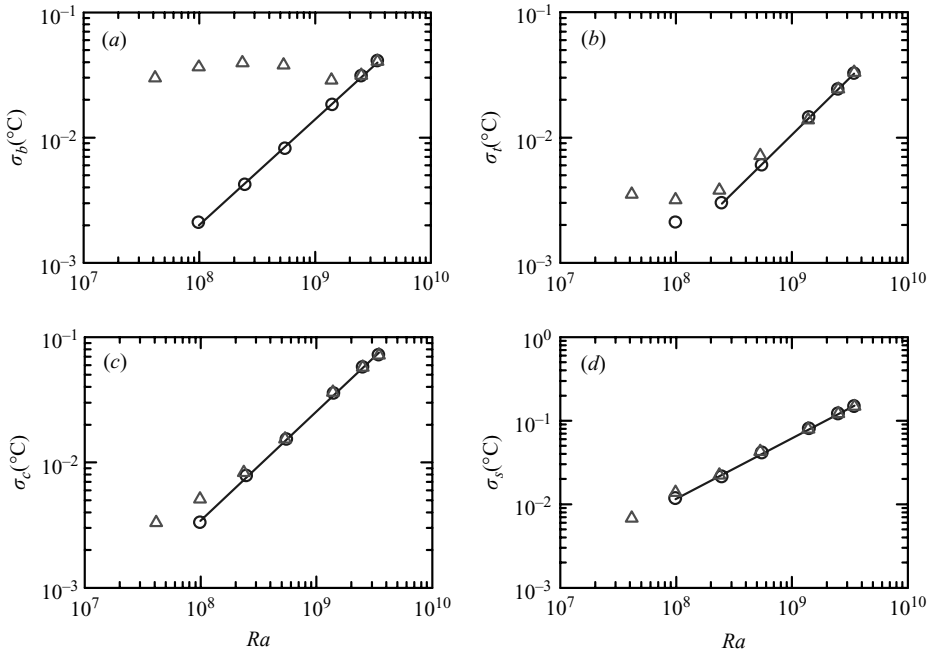

FIGURE 3. Standard deviations of local temperatures as a function of Ra measured at (*a*) bottom plate; (*b*) top plate; (*c*) cell centre; and (*d*) sidewall. Open triangles: pulsed heating ($\sigma^{(k)}$); open circles: constant heating ($\sigma^{(c)}$). Lines are power-law fits to the constant heating data.

The behaviour of $\sigma^{(k)}$ may be understood as the result of competition between two contributions: the modulation from the heating pulse and the stochastic turbulent fluctuations from convecting fluid such as plume emissions. At low Ra, stochastic turbulent fluctuations are weak and negligible when compared to the modulated temperature variations from the heating pulses. So the temperature fluctuation is dominated by the kicked heating and thus does not change much with the increase of Ra. At high Ra, the stochastic turbulent fluctuations are strong enough to overwhelm the contribution from the pulsed heating. Thus, the temperature fluctuation is dominated by the stochastic turbulent fluctuations, just like the constant heating case. As a result, $\sigma^{(k)}$ overlaps with $\sigma^{(c)}$ and increases with the increasing Ra. Since the pulsed heating power is directly fed to the lower plate, $\sigma_b^{(k)}$ is much more sensitive to the pulsed heating power than $\sigma_t^{(k)}$ and $\sigma_c^{(k)}$. This is probably the reason why the transition Ra for $\sigma_b^{(k)}$ is much higher than that for $\sigma_t^{(k)}$ and $\sigma_c^{(k)}$. In both pulsed and constant heating cases, most of the plumes pass through the sidewall region. Thus, compared to the conditions inside the plates and at the cell centre, the temperature fluctuations near the sidewall are much larger and so the contribution from turbulent fluctuations always overwhelms that from the modulated heating. This is probably the reason why the difference between $\sigma_s^{(k)}$ and $\sigma_s^{(c)}$ is very small.

To illustrate the above argument, we show in figure 4 three segments of steady-state local temperature time series measured inside the bottom plate for pulsed heating cases with fixed kicking strength $A = 347.66$ J and three different kicking frequencies. When f is low (figures 4*a* and 4*b*), the temperature is fully dominated by the pulsed heating. When f is high (figure 4*c*), the temperature in the bottom plate no longer

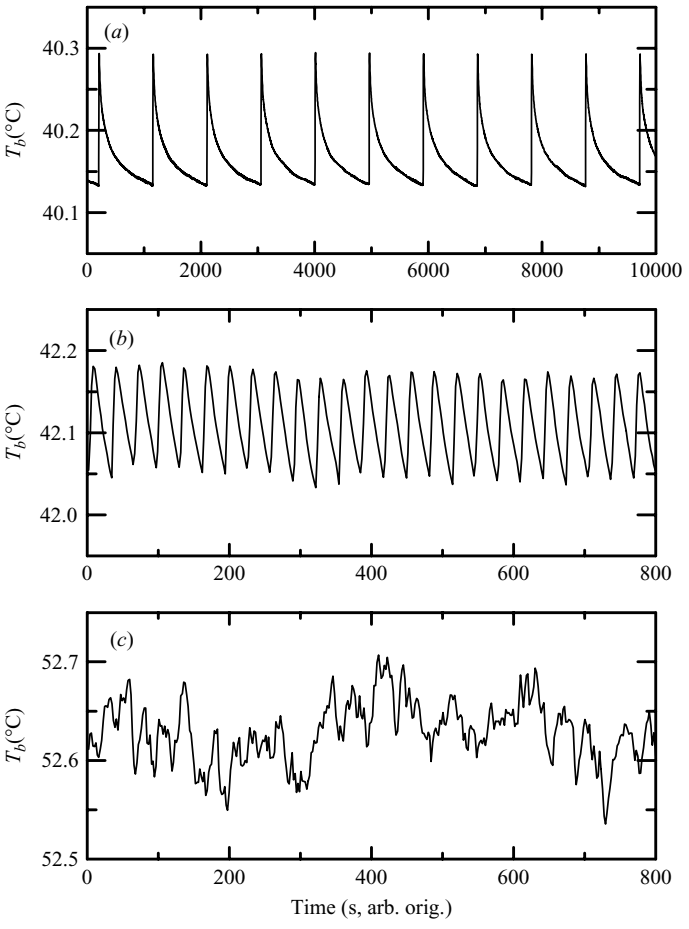

FIGURE 4. Segments of steady-state local temperature time series measured in the bottom plate for pulsed heating cases with fixed kicking strength $A = 347.66$ J and three different kicking frequencies (*a*) $f = 0.001$ Hz, (*b*) $f = 0.033$ Hz, and (*c*) $f = 0.5$ Hz.

follows the pulsed heating. It is mainly dominated by stochastic turbulent fluctuations from the fluid.

3.3. *The large-scale circulation (LSC)*

The existence of a large-scale circulatory flow or LSC is an important feature of steadily driven RBC. It was first observed by Krishnamurti & Howard (1981) and has been studied extensively in recent years. Many experimental, theoretical and numerical investigations have been carried out to study the various aspects of the LSC (see, for example, Xi, Zhou & Xia 2006, which contains a large compilation of relevant references). A natural question is, therefore, whether the LSC still exists in kicked RBC. To answer this, we measured the power spectra and the correlation functions of the temperature fluctuations near the sidewall of the convection cell.

Figure 5(*a*) shows the power spectra of mid-height sidewall temperature fluctuations for a pulsed heating case with pulse parameters $\Delta t = 88.1$ s, $\Delta t_{kick} = 2$ s, and $P = 173.83$ W. The corresponding constant heating case is also plotted for comparison. A weak peak located at $f_0 \sim 6 \times 10^{-3}$ Hz can be seen for both pulsed and constant heating cases. This suggests oscillations with characteristic frequency $f_0 \sim 6 \times 10^{-3}$

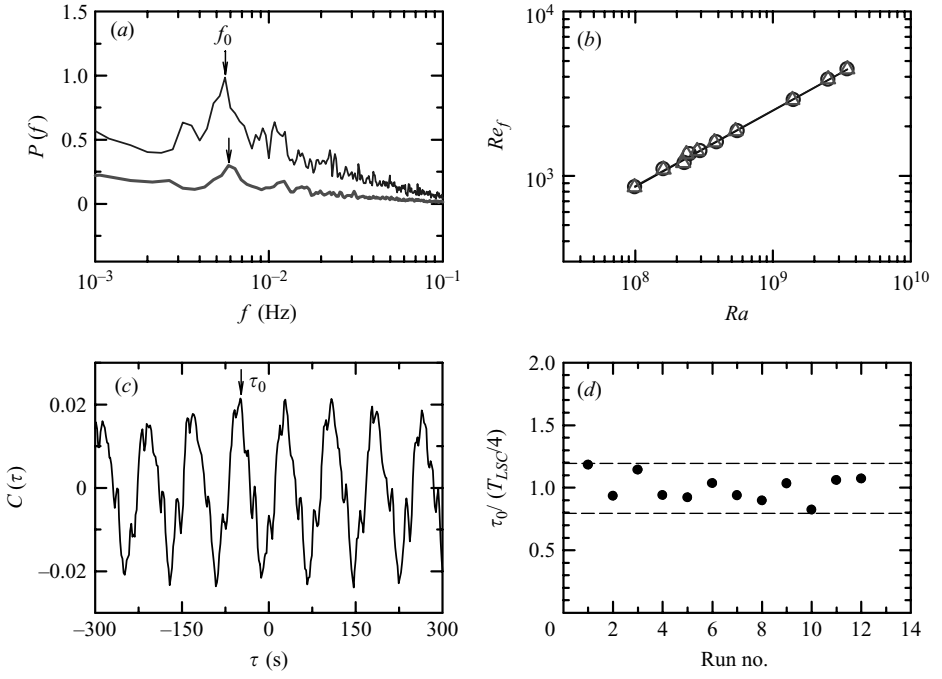

FIGURE 5. (*a*) Power spectra of temperature time series $T_s(t)$ measured near the sidewall at mid-height for a pulsed heating case with $\Delta t = 88.1$ s, $\Delta t_{kick} = 2$ s, $P = 173.83$ W (lower line) and its corresponding constant heating case. (*b*) Reynolds number Re_f as a function of Ra for pulsed (triangles) and constant (circles) heating cases. The solid lines are power-law fits. (*c*) Cross-correlation function between $T_s(t)$ and $P(t)$ for the pulsed heating case with $\Delta t = 88.1$ s, $\Delta t_{kick} = 2$ s, $P = 173.83$ W. τ_0 denotes the time-lag between $T_s(t)$ and $P(t)$. (*d*) Normalized time-lag τ_0 obtained from 12 measurements of pulsed heating cases.

Hz existing in the system. The fact that the oscillation frequency f_0 in the pulsed heating case is the same as that of the constant heating one is strong evidence that a large-scale circulatory flow also exists in the kicked RBC and it has the same turnover time $T_{LSC} = 1/f_0$ as the steadily driven RBC of equivalent heating power. We find that power spectra for other pairs of pulsed and constant heating cases have similar properties to those shown in figure 5(*a*). The circulation frequency f_0 may be used to define a Reynolds number of the LSC, i.e. $Re_f = 4H^2 f_0/\nu$. Figure 5(*b*) shows Re_f as a function of Ra for both pulsed and constant heating cases. The same power-law fit was obtained for both cases: $Re_f \propto Ra^{0.46\pm0.01}$. In fact, it is found that Re_f for each pair of constant and pulsed heating cases almost coincide with each other. These results show that the periodically kicked heating does not destroy LSC and that the LSC turnover time remains unchanged compared with the constant heating cases with the same saturated Ra. We have found that the LSC is maintained even when the kicking frequency ($f = 1/\Delta t$) is much smaller than the circulation frequency f_0. This means that, after a kick, the LSC can continue for many turnover times before another kick is needed to sustain it.

Figure 5(*c*) shows the cross-correlation function $C(\tau)$ between the pulsed heating power $P(t)$ and the mid-height sidewall temperature $T_s(t)$ for a pulsed heating case with pulse parameters $\Delta t = 88.1$ s, $\Delta t_{kick} = 2$ s, and $P = 173.83$ W. It is seen that the cross-correlation function has a periodic behaviour with a period equal to T_{kick},

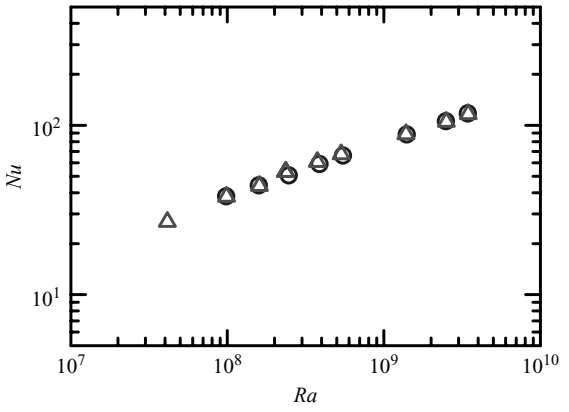

FIGURE 6. Nu as a function of Ra for both pulsed (triangles) and constant (circles) heating cases in the $\Gamma = 1$ cell.

indicating that overall the sidewall temperature is modulated by the pulsed heating. The location of the first peak on the left of the origin, denoted as τ_0, indicates the time-lag of $T_s(t)$ from $P(t)$. The peak was smoothed by polynomial fitting and the peak position was obtained to be $\tau_0 = -47$ s. Figure 5(d) shows $|\tau_0|$ obtained in more than ten experimental measurements with different pulse parameters. In the plot $|\tau_0|$ is normalized by a quarter of the LSC turnover time T_{LSC} obtained from the same measurement. This figure indicates that most of the measurements give $|\tau_0|$ in the range $(0.8 - 1.2)T_{LSC}/4$, which implies that it takes approximately $T_{LSC}/4$ to transport the pulsed heating power from the bottom plate to the mid-height point near the sidewall. This result reveals that in a convection system driven by kicked energy input, the boundary layer perturbation induced by the heating power is also transported by the LSC, just like in a steadily driven system described by the delayed coupling model (Villermaux 1995).

3.4. *Nusselt number enhancement*

Heat transport remains a central focus in the studies of turbulent thermal convection. In this section we examine how heat transport in kicked RBC compares to that in steadily driven RBC. The Nusselt number Nu_k for the kicked heating case and Nu_c for the corresponding constant heating case of equivalent heating power may be respectively defined as

$$Nu_k = \frac{\langle P(t)\rangle H}{\langle \Delta T(t)\rangle S\chi}, \tag{3.3}$$

$$Nu_c = \frac{P_c H}{\Delta T S\chi}, \tag{3.4}$$

where $\langle P(t)\rangle$ and $\langle \Delta T(t)\rangle$ are the time-averaged heating power and temperature difference respectively, and P_c is the heating power in the corresponding constant heating case: $P_c = P\Delta t_{kick}/(\Delta t_{kick} + \Delta t)$. S is the plate area. Figure 6 shows Nu_k and Nu_c as functions of Ra in a log-log plot. It is seen that at the resolution of the plot there appears to be little difference in Nusselt number between the pulsed and constant heating cases. If we make a power-low fit to the measured data, we obtain an exponent of about 0.3. As we have not attempted to correct the heat leakages through the sidewall and the bottom of the cell, we will not make any further quantitative analysis of the behaviour of Nu. Our objective here is to compare the relative heat

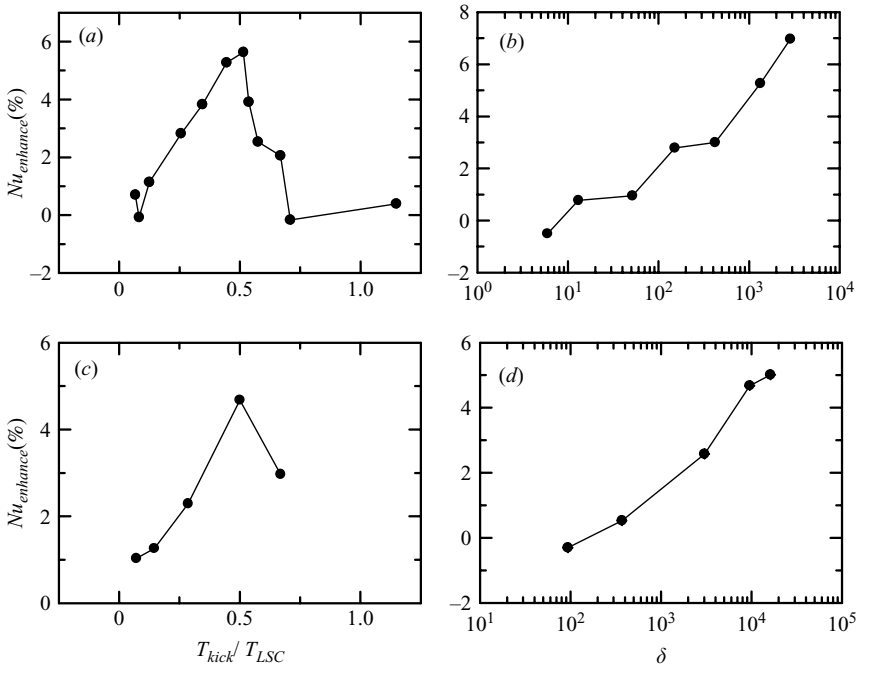

FIGURE 7. (a, c) $Nu_{enhance}$ as a function of the normalized pulse repetition period T_{kick}/T_{LSC} with a fixed pulse shape index. (b, d) $Nu_{enhance}$ as a function of the pulse shape index δ with a fixed pulse repetition period. (a, b) Data from the $\Gamma = 1$ cell and (c, d) the $\Gamma = 0.5$ cell. In (a) and (c) $\delta = 2029.5$ and 9604, respectively. In (b) and (d) $T_{kick} = 73$ s and 196 s, respectively.

transport efficiency (the Nusselt number) between the kicked and steadily driven cases under otherwise identical conditions. For this, we define the Nusselt number enhancement as

$$Nu_{enhance} = \frac{Nu_k - Nu_c}{Nu_c}. \tag{3.5}$$

Figure 7 shows Nusselt number enhancement for kicked RBC, with the upper panels showing data measured in the $\Gamma = 1$ cell and the lower panels those from the $\Gamma = 0.5$ cell. All the pulsed heating measurements were made with the same kicking strength A, i.e. the same energy contained in each pulse. The average values of Ra varied from 1×10^8 to 3×10^9 for $\Gamma = 1$ and those for $\Gamma = 0.5$ varied from 7×10^8 to 2×10^{10}. Figure 7(a) shows $Nu_{enhance}$ as a function of pulse repetition period T_{kick} $(= \Delta t_{kick} + \Delta t)$ with fixed pulse shape. Here T_{kick} is normalized by the LSC turnover time T_{LSC}; and Δt_{kick} and P were fixed to be 2 s and 173.83 W, respectively. The figure indicates that pulsed heating leads to an enhancement in Nusselt number within an appropriate range of T_{kick} and that when $T_{kick} \approx T_{LSC}/2$, a resonance occurs, i.e. the enhancement is optimized. When T_{kick} deviates from $T_{LSC}/2$, $Nu_{enhance}$ decreases and eventually goes down to zero. Now that we have found the pulsed heating is more efficient for heat transport, it is interesting to know whether the enhancement depends on the shape of the pulse, i.e. would a spiky pulse be more efficient for heat transfer than a flatter one of the same energy, or vice versa? Here we define a dimensionless 'pulse shape index' δ as

$$\delta = \frac{P/\Delta t_{kick}}{P_c/T_{kick}} = \left(\frac{T_{kick}}{\Delta t_{kick}}\right)^2. \tag{3.6}$$

It is a measure of the difference in pulse shape between the pulsed heating and the corresponding constant heating case. Note that the right-hand side of (3.6) is related to the duty cycle $C = \Delta t_{kick}/(\Delta t_{kick} + \Delta t) = \Delta t_{kick}/T_{kick}$ of energy input, i.e. $\delta = 1/C^2$. A large δ (or a small duty cycle) means a tall thin pulse and the forcing is more different from the constant heating case. On the other hand, a small δ means a short fat pulse, and the limiting case of δ approaching to 1 corresponds to constant heating. Figure 7(*b*) shows $Nu_{enhance}$ as a function of δ for a fixed repetition period $T_{kick}(= 73$ s). In the figure, all data points have the same kicking strength A so that the pulses of varying shape all contain the same amount of energy. Clearly, there is a monotonic increase of $Nu_{enhance}$ with increasing δ (or with decreasing duty cycle). For our present apparatus, the largest value of the shape index that can be achieved for the $\Gamma = 1$ cell is $\delta = 2856$ (corresponding to a duty cycle of 1.9%), which gives rise to $Nu_{enhance}$ of about 7%. When δ decreases to the order of 10 ($C \approx 30\%$), no appreciable Nusselt enhancement was found. Similar properties are found for the $\Gamma = 0.5$ cell, which are shown in figures 7(*c*) and 7(*d*). For this cell, $Nu_{enhance}$ achieves a maximum value of 4.7% at $T_{kick} = T_{LSC}/2$ for a fixed pulse shape and a maximum value of about 5% at $\delta = 16227.5$ ($C \approx 0.8\%$) for a fixed repetition period. These results suggest that the most efficient heat transfer is achieved when the pulse takes a δ-function-like shape or a duty cycle approaches zero.

The dependence of $Nu_{enhance}$ on the pulse repetition period T_{kick} for a fixed pulse shape may be understood in terms of the interplay between plume emissions and the large-scale circulation. As shown in § 3.3, the LSC still exists in kicked RBC and the thermal plumes are also transported by the LSC in kicked thermal turbulence. Moreover, as shown in figure 5(*d*), it takes about a quarter of the LSC turnover time for the plumes emitted from the plates to reach the mid-height of the sidewall. When combining these results with the delayed-coupling model of Villermaux (1995), a simple physical picture of kicked thermal turbulence can be sketched. There are two time scales in the system: pulsed heating period T_{kick} and LSC turnover time T_{LSC}. The cell crossing time T_0 is related to the LSC turnover time: $T_0 = T_{LSC}/2$ (Villermaux 1995; Sun, Xia & Tong 2005). At the lower plate, boundary layer perturbation is mainly produced by the heating pulses, and thus has the period of T_{kick} and thermal plumes triggered by boundary layer perturbations are transported by the LSC. After a time $T_{LSC}/2$, plumes emitted in the lower boundary layer have been transported to the upper boundary layer. In other words, the emission of thermal plumes is dictated by pulsed heating (with period T_{kick}), while the transportation of thermal plumes is dictated by the LSC (with period T_{LSC}). When $T_{kick} = T_{LSC}/2$, the plume emission period just matches the time needed for the plume to reach the upper plate. This means that at the moment the first cluster of plumes reaches the upper plate the subsequent cluster of plumes is being emitted at the bottom plate. It seems that this synchronized plume emission and transportation is the most efficient way of heat transfer in the RBC system.

The shape index dependence of $Nu_{enhance}$ for a fixed pulse repetition period may be understood as follows. A small δ corresponds to a flatter pulse or a large duty cycle; with T_{kick} fixed this means that the heating approaches a steadily driven case and $Nu_{enhance}$ should be zero. When δ increases (with A and T_{kick} fixed), a more intense and spiky pulse is generated, which should produce a larger perturbation to the boundary layer compared to a steadily driven case. As plumes are presumably produced by boundary layer instabilities, this implies that a spiky pulse is more efficient in inducing the release of plumes from the boundary layer and these plumes are more likely to form clusters as they are all generated within a short period of time.

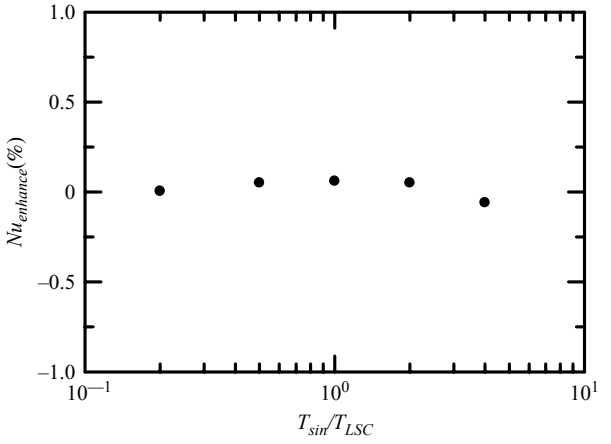

FIGURE 8. The relative Nu change $Nu_{enhance}$ measured in an $\Gamma = 1$ convection cell with a sinusoidally modulated heating power input. Here the modulation period T_{sin} is normalized by the LSC turnover time T_{LSC}.

When the plumes cluster together they should be more efficient in transporting heat, as they will suffer less heat loss to the surrounding fluid through diffusion. Therefore, there is an increase in Nu_k when δ increases (or duty cycle decreases). As all the pulsed heating cases with varying δ have the same corresponding constant heating, Nu_c remains the same when δ increases. Therefore, $Nu_{enhance}$ increases monotonically with δ. Thus, spiky pulses are more efficient for heat transfer than flatter pulses of the same energy. In other words, the more the type of forcing is different from the constant forcing, the more efficient is the heat transfer rate. Our results also show that a small duty cycle is more efficient than a larger one, i.e. the heater should stay idle for most of the time and then give the system an intense pulse (kick) for maximum efficiency.

We also conducted a modulated RBC experiment, in which the system is driven by a sinusoidally varying power input. The experiment was made at $Ra = 3 \times 10^9$ for which $T_{LSC} \approx 50$ s. The (power) modulation amplitude to offset ratio is 1 and the modulation period T_{sin} varied from 10 s to 200 s. The result is shown in figure 8, where it is seen that no appreciable Nusselt number enhancement is detected within the experimental resolution. This result further confirms the effect of forcing shape on Nusselt number enhancement. Since the effective pulse shape index of a sinusoidal power input is small ($\delta \sim 4$, which corresponds to a large duty cycle of $C \sim 50\%$), it is reasonable that sinusoidal forcing cannot induce a Nusselt number enhancement.

In summary, whether a specific pulsed heating can produce Nusselt number enhancement depends on two factors. One is the synchronization between the period of the pulsed heating and the intrinsic time scale (e.g. LSC turnover time) of the turbulent flow. In our system, when the pulse repetition period equals half a LSC turnover time, i.e. $T_{kick} = T_{LSC}/2$, a resonance occurs and the enhancement is optimized. The other factor is the pulse shape (or the duty cycle of energy input): sharp pulses (or small duty cycles) are better for heat transfer than flatter ones of the same energy. Obviously, if the LSC breaks down at much higher values of Ra, the part of Nusselt number enhancement due to the synchronization with the LSC turnover time is expected to be diminished. On the other hand, the part due to enhanced emission of clustered plumes, induced by spiky pulses, should still be present.

3.5. *A mean-field theory for kicked thermal turbulence*

Our results in § 3.1 may be understood more quantitatively by modifying Lohse's mean-field theory to the case of kicked thermal turbulence. Therefore, the derivations below follows closely that of Lohse (2000), except for places that are particular for thermal turbulence.

Because the Rayleigh number plays a similar role in thermal turbulence as the Reynolds number does in shear flow turbulence, we aim to find a relationship between Ra^{sat} and A and f similar to that between Re^{sat} and A and f derived by Lohse. For thermally driven turbulent flows, the viscous dissipation rate depends on Ra, Pr, and Nu (see, for example, Shraiman & Siggia 1990):

$$\varepsilon = \frac{\nu^3 Pr^{-2} Ra(Nu-1)}{H^4} \approx \frac{\nu^3 Pr^{-2} RaNu}{H^4}. \tag{3.7}$$

By neglecting the heat loss:

$$\varepsilon = \frac{g\alpha\kappa P}{S\chi} = \frac{g\alpha P}{S\rho C_p}, \tag{3.8}$$

where P is the heating power applied to the lower plate, S is the area of the plate, and ρ and C_p are respectively the density and the specific heat of the convecting fluid (the other quantities have already been defined in § 1). To study a convection system driven by a pulsed heating power, two issues should be first investigated: the energy input during the pulse activation time; and the energy decay during the time between two successive pulses. When a pulse is fed to the lower plate, there should be an energy increase proportional to the dissipation rate,

$$\dot{E}(t) = \beta\varepsilon = \beta\frac{g\alpha P}{S\rho C_p} = \xi P, \tag{3.9}$$

where P is now the pulse height, β is an unknown proportionality constant and $\xi = \beta g\alpha/(S\rho C_p)$. After a pulse input the initial energy E_0 increases to E_1,

$$E_1 \approx E_0 + \dot{E}(t)\Delta t_{kick} = E_0 + \xi P \Delta t_{kick} = E_0 + \xi A. \tag{3.10}$$

A Reynolds number based on the r.m.s. velocity can be defined as (Lohse 2000)

$$Re(t) = \frac{Hu_{rms}}{\nu} = \frac{H\sqrt{2E(t)}}{\nu}. \tag{3.11}$$

Then (3.10) can be rewritten as

$$Re_1 = Re_0\sqrt{1 + \frac{2H^2\xi A}{\nu^2 Re_0^2}}. \tag{3.12}$$

Equation (3.12) indicates a kick in Reynolds number from Re_0 to Re_1 when a pulse of power is fed to the system. It determines the evolution of Reynolds number or energy during the pulse activation time. Between two successive pulses, the turbulent activity decays and the Reynolds number evolves from an initial value of Re_i to a value $Re(t)$ in time t according to the following inverse function (Lohse 2000):

$$\frac{t(Re)}{\tau} = \frac{3}{c_{\varepsilon,\infty}}[F(Re) - F(Re_i)], \tag{3.13}$$

where $F(Re)$ is given by

$$F(Re) = \frac{1}{2Re^2}\left(-\gamma + \sqrt{\gamma^2 + Re^2}\right) + \frac{1}{2\gamma}\ln\left(\frac{\gamma + \sqrt{\gamma^2 + Re^2}}{Re}\right). \tag{3.14}$$

In the above $c_{\varepsilon,\infty}$ is the dimensionless energy dissipation in the large Reynolds number limit, γ is inversely related to $c_{\varepsilon,\infty}$, and both constants are of order 1 (Lohse 2000). Obviously, (3.12)–(3.14) with $0 \leqslant t \leqslant \Delta t$ can fully describe the time evolution of the Reynolds number. During each cycle there is a kick in Reynolds number from Re_0 to Re_1 according to (3.12) and a subsequent decay according to (3.13) and (3.14). The Reynolds number will overall increase until the energy input from a pulse in Δt_{kick} balances the energy loss through decay in Δt. A steady state is then achieved in which the Reynolds number fluctuates between a lower level Re_l^{sat} and an upper level Re_u^{sat}, which should satisfy (3.12), i.e.

$$Re_u^{sat} = Re_l^{sat}\sqrt{1 + \frac{2H^2\xi A}{\nu^2 (Re_l^{sat})^2}}. \tag{3.15}$$

Because the system decays from Re_u^{sat} to Re_l^{sat} during one kicking period $(1/f)$, according to (3.13) the two levels should also satisfy

$$\frac{1}{\tau f} = \frac{3}{c_{\varepsilon,\infty}}\left[F(Re_l^{sat}) - F\left(Re_l^{sat}\sqrt{1 + \frac{2H^2\xi A}{\nu^2 (Re_l^{sat})^2}}\right)\right]. \tag{3.16}$$

The above two equations give the relationship between the saturation levels of the Reynolds number and the two control parameters, the kicking strength A and kicking frequency f. To make a more direct comparison with experimental results, we simplify the above relationships to deduce scaling relations between Re and A and f. As argued by Lohse (2000), a turbulent regime occurs when Re_l^{sat}, $Re_u^{sat} \gg \gamma$. This should occur for large enough values of A and f. When this is satisfied, (3.14) becomes $F(Re) \approx 1/2Re$. In turn, (3.16) can be simplified as

$$\frac{1}{\tau f} = \frac{3}{2c_{\varepsilon,\infty}}\left(\frac{1}{Re_l^{sat}} - \frac{1}{Re_l^{sat}\sqrt{1 + 2H^2\xi A/[\nu^2 (Re_l^{sat})^2]}}\right), \tag{3.17}$$

$$\frac{1}{\tau f} \propto \frac{\sqrt{1 + 2H^2\xi A/[\nu^2 (Re_l^{sat})^2]} - 1}{Re_l^{sat}\sqrt{1 + 2H^2\xi A/[\nu^2 (Re_l^{sat})^2]}}. \tag{3.18}$$

If we further assume that $2H^2\xi A/[\nu^2 (Re_l^{sat})^2] \ll 1$, (3.18) can be simplified as

$$\frac{1}{\tau f} \propto \frac{H^2\xi A}{\nu^2 (Re_l^{sat})^2}/Re_l^{sat} \propto \frac{A}{(Re_l^{sat})^3}. \tag{3.19}$$

Consequently,

$$Re_l^{sat} \propto (Af)^{1/3}, \tag{3.20}$$

$$Re_u^{sat} \sim Re_l^{sat} \propto (Af)^{1/3}, \tag{3.21}$$

where the last step comes from (3.15). This result shows that in kicked thermal turbulence both Re_u^{sat} and Re_l^{sat} scale with the product of Af to a power of 1/3. In Lohse (2000) a different exponent was obtained for shear flow turbulence. This is because the relationship between the dissipation rate ε and the kicking strength A is

different in the two cases. But, as pointed out by Lohse, the essential result is that the saturation levels scale with the product of Af.

With the Reynolds numbers obtained above, we can deduce the Rayleigh number evolution in kicked thermal turbulence using the relationship between Ra and Re. A previous experiment (Lam *et al.* 2002) has measured the relation between Re and Ra in steadily driven RBC: $Re_{rms} \propto Ra^{0.40\pm0.03}$. Here we assume that this relationship still holds in the case of kicked RBC. Although Re_{rms} was not measured in kicked RBC, in § 3.2 we showed that the Reynolds number based on the circulation frequency (f_0) of the large-scale flow in kicked RBC has the same power-law dependence on Ra as in steadily driven RBC, i.e. $Re_f \propto Ra^{0.46\pm0.01}$, where $Re_f = 4H^2 f_0/\nu$. Thus Ra should also have an overall growth to a saturation level and the saturated $Ra(t)$ should fluctuate between a lower saturation level Ra_l^{sat} and an upper saturation level Ra_u^{sat}, and these features are confirmed by the experimental results (figure 1). If we use the relationship $Re_{rms} \propto Ra^{0.40\pm0.03}$ (Lam *et al.* 2002), a power-law dependence between the saturation levels of Ra and the product Af can be established:

$$Ra_l^{sat},\ Ra_u^{sat} \propto (Af)^{0.83\pm0.07}. \tag{3.22}$$

However, if the circulation-frequency-based Reynolds number $Re_f \propto Ra^{0.46\pm0.01}$ is used, we would instead have a different scaling:

$$Ra_l^{sat},\ Ra_u^{sat} \propto (Af)^{0.72\pm0.03}. \tag{3.23}$$

Comparing these results with the experimental findings from § 3.1, i.e. $Ra_l^{sat} \propto (Af)^{0.80\pm0.02}$ and $Ra_u^{sat} \propto f^{0.70\pm0.01}A^{0.84\pm0.02}$, we see that (3.22), within the experimental uncertainties, has a quantitative agreement with the experiment (at least for Ra_l^{sat}). Indeed, it is the r.m.s.-velocity-based Reynolds number that was used in the original mean-field theory. And here we see that this choice of Reynolds number is supported by the experimental result.

The above also shows that the agreement between experiment and theory for Ra_u^{sat} is less than satisfactory. We now discuss the possible reasons for this discrepancy and the limitations of the scaling result. The predicted scaling result is based on the requirement

$$X \equiv \frac{2H^2\xi A}{\nu^2(Re_l^{sat})^2} \ll 1. \tag{3.24}$$

This implies a small enough kicking strength A and a large enough lower saturation level Re_l^{sat}. However, Re_l^{sat} also depends on A and f. Substituting $Re_l^{sat} \propto (Af)^{1/3}$ into (3.24), we have

$$X \sim A^{0.33} f^{-0.67} \ll 1. \tag{3.25}$$

Therefore, generally speaking, A should be small enough and f should be large enough to satisfy the requirement $X \ll 1$ so that (3.21) can be established. However, when f is too large, the pulsed heating will approach the limiting case that the lower plate is continuously heated by a constant heating power with amplitude equalling the pulse height P. Thus the saturation level of Ra will no longer increase and (3.21) (and thus (3.22)) will break down. On the other hand, large enough A and f are also required for the flow to stay in the turbulent regime and for Ra to reach a saturation level. These analyses indicate that the power-law regime exists only for appropriate ranges of f and A. This is consistent with our experimental results (figure 2) which reveal that a power-law dependence of Ra_l^{sat} and Ra_u^{sat} on A and f exists only when Ra^{sat} is larger than 10^8.

Regarding the less-than-quantitative agreement between the experimentally determined scaling behaviour and the mean-field prediction for Ra_u^{sat}, a possible reason for this is that a more stringent condition for the validity of the scaling regime is required for Ra_u^{sat} than for Ra_l^{sat}. From (3.15) we see that in order for Re_u^{sat} and Re_l^{sat} (therefore, Ra_u^{sat} and Ra_l^{sat}) to exhibit the same scaling behaviour (3.24) must be satisfied, i.e. $X \ll 1$. Thus, although (3.24) is the condition for the validity of the scaling result (3.20) (which leads to the scaling of both Ra_l^{sat} and Ra_u^{sat}), the scaling of Ra_u^{sat} appears to have a more sensitive dependence on this condition via (3.15). Using the measured Re and (3.17) the value of X can be obtained. The result shows that (3.24) is in fact not satisfied for most values of the kicking strength A and it is satisfied only for some of the highest values of the kicking frequency f used in the present experiment (note, however, that some of the constants used in the estimation of X, like the dimensionless energy dissipation $c_{\varepsilon,\infty}$, are those for classical shear flows and they may be different for turbulent convection). On the other hand, this result may be taken to imply that the scaling of Re_l^{sat} as a product of A and f in kicked thermal turbulence is a more robust feature than is suggested in the simple mean-field theory. It should also be mentioned that the original mean-field theory requires $\Delta t_{kick} \ll \Delta t$, which is not always satisfied in our experiment. This may mean that some of the conditions in the theory could be less restrictive.

In summary, when appropriately extended to the case of thermal turbulence, the mean-field theory of kicked turbulence first proposed by Lohse can explain our experimental results. To the best of our knowledge, the present study is also the first experimental verification of Lohse's mean-field theory. Specifically, our experiment verifies the two main predictions of mean-field theory: first, the saturated $Re(t)$ ($Ra(t)$ in our system) fluctuates between a lower saturation level and an upper saturation level; second, for large Re (Ra), the saturation levels scale as the product of Af.

4. Conclusion

We have performed a periodically kicked turbulence experiment in the Rayleigh–Bénard convection (RBC) system and investigated the impact of this specific type of forcing on turbulent convective flows and heat transport. Four major findings are summarized below:

(i) For appropriate ranges of the kicking strength A and the kicking frequency f, $Ra(t)$ has an overall growth to a saturation level and the saturated $Ra(t)$ oscillates between a lower saturation level Ra_l^{sat} and an upper saturation level Ra_u^{sat}.

(ii) For sufficiently large values of $Ra^{sat}(\sim 10^8)$, the saturation levels have power-law dependence on A and f: $Ra_l^{sat} \propto (Af)^{0.80\pm0.02}$ and $Ra_u^{sat} \propto f^{0.70\pm0.01}A^{0.84\pm0.02}$. It is found that the scaling of Ra_l^{sat} agrees quantitatively with the theoretical prediction of a mean-field theory when the latter is appropriately modified for kicked thermal turbulence.

(iii) We have found evidence that a large-scale circulatory flow (LSC) still exists in the kicked RBC, just as in the steadily driven case. It is also found that the LSC has the same flow strength in both the kicked and steadily driven cases and that the Reynolds number based on the circulation frequency of the LSC scales with Ra as $Re_f \propto Ra^{0.46\pm0.01}$, which, within experimental resolution, is the same as that of the steadily driven case.

(iv) A kicked energy input enhances the Nusselt number when appropriate pulse parameters are selected. Moreover, a resonance in the enhancement is found when the input pulse period is synchronized with half of the large-scale flow turnover time. For

the apparatus used in our system, a maximum enhancement of about 7% is obtained. In principle, this value could be larger with appropriate instrument, for example, when a power supply capable of producing a more intense pulse is used. We find that whether a specific pulsed heating can produce Nusselt number enhancement depends on two factors. One is the synchronization between the period of the pulsed heating and the intrinsic time scale (e.g. LSC turnover time) of the turbulent flow. When the pulse repetition period equals half of the LSC turnover time, i.e. $T_{kick} = T_{LSC}/2$, the enhancement is optimized. The other factor is the pulse shape (or duty cycle). It is found that a spiky pulse is more efficient for heat transport across the convection cell than a tubby one of the same energy. This result implies that the most efficient heat transfer is achieved when a δ-function-like pulse is used. Physically, we think this enhancement is related to a more effective release of clustered thermal plumes, as the plumes are known to be the main carriers of heat in the RBC system. This is because an intense and spiky pulse can perturb the boundary layer more effectively than constant heating and so can more efficiently induce the emission of large clusters of thermal plumes. Furthermore, when the plumes cluster together they should be more efficient in transporting heat, as they will suffer less heat loss to the surrounding fluid through diffusion. When the release of large clusters of thermal plumes is further synchronized with the LSC turnover time, an enhanced heat transfer is achieved. Our finding also reveals a mechanism to appropriately design the forcing type so that more efficient heat transport in the convective turbulence system can be achieved. In contrast, a sinusoidally modulated energy input is found to produce no detectable enhancement of heat transfer.

The present work is the first, and a preliminary, experimental investigation of kicked turbulent flows. There are obviously many issues to be addressed in future studies. For example, the long period between kicked energy inputs ($1/f \sim$ few hundred seconds) provides with us the opportunity to study intermittency effects in free decaying turbulence in a thermal convection system, which may provide insight into energy cascades in turbulent flows. The other interesting issue is the long decay time of the flow, i.e. the large-scale flow can still be maintained (on average) when the kicking period (T_{kick}) is much larger than the LSC turnover time (T_{LSC}). This suggests that the LSC is really a robust phenomenon with an intrinsic time scale that is still not well understood. The enhanced heat transport is also a surprise finding and may have applications.

It is a pleasure to acknowledge helpful discussions with D. Lohse and support of this work by the Research Grants Council of Hong Kong SAR under Grant No. CUHK403705 and CUHK403806.

REFERENCES

Cadot, O., Titon, J. H. & Bonn, D. 2003 Experimental observation of resonances in modulated turbulence. *J. Fluid Mech.* **485**, 161–170.

von der Heydt, A., Grossmann, S. & Lohse, D. 2003*a* Response maxima in modulated turbulence. *Phys. Rev.* E **67**, 046308.

von der Heydt, A., Grossmann, S. & Lohse, D. 2003*b* Response maxima in modulated turbulence. II. Numerical simulations. *Phys. Rev.* E **68**, 066302.

Hooghoudt, J.-O, Lohse, D. & Toschi, F. 2001 Decaying and kicked turbulence in a shell model. *Phys. Fluids* **13**, 2013–2018.

Krishnamurti, R. & Howard, L. N. 1981 Large-scale flow generation in turbulent convection. *Proc. Natl Acad. Sci. USA* **78**, 1981–1985.

Kuczaj, A. K., Geurts, B. J. & Lohse, D. 2006 Response maxima in time-modulated turbulence: Direct numerical simulations. *Europhys. Lett.* **73**, 851–857.

Lam, S., Shang, X.-D., Zhou, S.-Q. & Xia, K.-Q. 2002 Prandtl number dependence of the viscous boundary layer and the Reynolds numbers in Rayleigh-Bénard convection. *Phys. Rev.* E **65**, 066306.

Lohse, D. 2000 Periodically kicked turbulence. *Phys. Rev.* E **62**, 4946–4949.

Shang, X.-D., Qiu, X.-L., Tong, P. & Xia, K.-Q. 2003 Measured local heat transport in turbulent Rayleigh-Bénard convection. *Phys. Rev. Lett.* **90**, 074501.

Shang, X.-D. & Xia, K.-Q. 2001 Scaling of the velocity power spectra in turbulent thermal convection. *Phys. Rev.* E **64**, 065301(R).

Shraiman, B. I. & Siggia, E. D. 1990 Heat transport in high-Rayleigh-number convection. *Phys. Rev.* A **42**, 3650–3653.

Sun, C. & Xia, K.-Q. 2007 Multi-point local temperature measurements inside the conducting plates in turbulent thermal convection. *J. Fluid Mech.* **570**, 479–489.

Sun, C., Xia, K.-Q. & Tong, P. 2005 Three-dimensional flow structures and dynamics of turbulent thermal convection in a cylindrical cell. *Phys. Rev.* E **72**, 026302.

Villermaux E. 1995 Memory-induced low frequency oscillations in closed convection boxes. *Phys. Rev. Lett.* **75**, 4618–4621.

Xi, H.-D., Lam, S. & Xia, K.-Q. 2004 From laminar plumes to organized flows: the onset of large-scale circulation in turbulent thermal convection. *J. Fluid Mech.* **503**, 47–56.

Xi, H.-D., Zhou, Q. & Xia, K.-Q. 2006 Azimuthal motion of the mean wind in turbulent thermal convection. *Phys. Rev.* E **73**, 056312.